MATERIALS SELECTION IN ELECTROMAGNETIC LAUNCHER DESIGN

E. P. Fahrenthold

Presented at the
Symposium on Advances in Mechanical Behavior
and Properties Evaluations
Winter Annual Meeting of The American Society
of Mechanical Engineers

Chicago, Illinois
November 27 to December 2, 1988

Publication No. PN-137
Center for Electromechanics
The University of Texas at Austin
Balcones Research Center
EME 1.100, Building 133
Austin, TX 78758-4497
(512)471-4496

MATERIALS SELECTION IN ELECTROMAGNETIC LAUNCHER DESIGN

E. P. Fahrenthold
Center for Electromechanics
University of Texas
Austin, Texas

The design of electromagnetic launchers includes a large materials selection component, with the use of available structural materials constrained by electrical performance considerations. Feasible material combinations for the composite structure are limited, with mechanical and thermo-electromagnetic simulations required to compare the performance of alternative designs. Numerical modeling studies suggest that next generation devices constructed for laboratory facilities or vehicular mounting may differ markedly in material composition, yet offer similar and significant structural improvements over conventional railgun designs.

NOMENCLATURE

B = magnetic flux density, Wb/m^2
c = specific heat per unit voulume, $J/(^oC\text{-}m^3)$
c_o = specific heat per unit volume at ambient temperature, $J/(^oC\text{-}m^3)$
c' = rate of change of the specific heat per unit volume with temperature, $[J/(^oC\text{-}m^3)]/^oC$
E = electric field intensity, V/m; or Young's modulus, Pa
h = rail half-thickness, m
H = magnetic field intensity, A/m
I = current, A
J = current density, A/m^2
k = thermal conductivity, $W/(m\text{-}^oC)$
k_o = thermal conductivity at ambient temperature, $W/(m\text{-}^oC)$
k' = rate of change of the thermal conductivity with temperature, $[W/(m\text{-}^oC)]/^oC$
p = duration of a current pulse, sec
t = time, sec
T = temperature, ^oC
T_o = ambient temperature, ^oC
U = internal energy per unit volume, J/m^3
w = rail perimeter, m
y = distance from the rail surface, m
μ = magnetic permeability, H/m
ν = Poisson's ratio
ρ = resistivity, ohm-m
ρ_o = resistivity at ambient temperature, ohm-m
ρ' = rate of change of the resistivity with temperature, $ohm\text{-}m/^oC$

INTRODUCTION

The mechanical design of electromagnetic launchers may be characterized as a complex pressure vessel design problem incorporating dynamic and asymmetric internal pressure loading and an unusual combination of electromagnetic, thermal, manufacturing, and assembly constraints. The structural design process for such a device includes a large materials selection component, with the identification of feasible structural materials and the quantification of weight or cost versus performance trade-offs dependent upon computer aided design techniques.

With a recent revival of interest in hypervelocity impact phenomena for equation of state, micrometeorite impact, and kinetic energy penetrator research (Johnson, 1987), the efficient design of electromagnetic launchers is currently under study at a number of government and commercial facilities. Although detailed finite element models of prototype launchers have been analyzed (Davidson et al., 1986), there remains a need for improvements in the integrated electromechanical design of these devices. Hence this paper considers the important role of materials selection in the design process for such systems, with a focus on the use of numerical modeling in feasibility and performance studies.

MECHANICAL DESIGN

Structural geometry and applied loads

The operation of a railgun is described in standard texts (Brown and Hamilton, 1984) and other references (Weldon, 1987) and hence will not be detailed here. These devices are in essence very specialized translational (as opposed to rotational) electric motors which use capacitive or inductive energy stores to accelerate solid projectiles to very high velocities. The component parts of a typical railgun structure are depicted in the cross sectional schematic of Figure 1. This compound pressure vessel consists of: (1) current conducting rails along which the armature or projectile slides, (2) nonconduting sidewalls which separate the rails and form a plasma seal for the bore, (3) an inner structural member which maintains the desired rail geometry under operating loads, (4) an outer structural member which provides preloading and longitudinal stiffness, and (5) a fluid or epoxy layer which may be located between the inner and outer structural members to provide a preloading capability and in some cases allow for convenient disassembly. In the interest of brevity and a focus upon material properties effects, the discussion which follows is limited to circular structual geometries of the type shown in Figure 1. Although square bores and a variety of rail support systems have

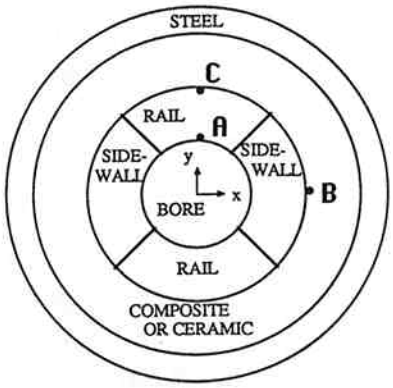

Figure 1. Cross sectional schematic of a round bore electromagnetic launcher.

been employed in practice, the materials selection issues considered here are generally representative of those encountered in all electromagnetic launcher design studies.

The highly transient Lorentz body force which acts upon the rails during firing is normally modeled as a uniform time dependent boundary pressure applied to the rails behind the projectile and along the bore surface. Although this conventional loading simplification may not accurately describe the stress distribution in the rail material, it does properly characterize the important asymmetric nature of the rail repulsion loads applied to the support structure. Since the duration of the applied load typically varies between one and ten milliseconds, inertial effects can be important to structural response predictions. However previous work (Fahrenthold et al., 1988a) has shown that fundamental comparisons of strength and stiffness properties of alternative mechanical designs may be made on the basis of static finite element analyses. Hence the only transient modeling results presented here are of the electromagnetic type.

In addition it should be noted that since current flows only to the rear of the projectile or armature, the relevant mechanical and electromagnetic modeling problems are inherently three dimensional. Although Fahrenthold et al. (1988b) have shown that three dimensional mechanical effects such as longitudinal bending are generally of secondary design importance, the author is not aware of any general treatment of the corresponding nonlinear three dimensional current diffusion problem.

The following paragraphs discuss materials selection alternatives for various components of the system.

Inner supporting structure

The inner supporting structure provides primary containment for the rail-sidewall assembly. Since the overall system weight and stiffness is generally a strong function of this component's design, its composition and configuration determines to a large extent the launcher's mechanical efficiency. Although the inner support structure performs a strictly mechanical function, its design is subject to two important electrical constraints. It must not allow short circuiting of the launcher's rails and it must not support the generation of eddy currents during the highly transient input power pulse. These constraints are typically met by fabricating the inner structure of nonconducting materials, a solution which presently incorporates significant weight or stiffness penalties.

Practical candidate materials for a nonconducting inner support structure are limited to ceramics and fiber reinforced composites. To date most electromagnetic launcher designs have incorporated fiber reinforced composites in the inner supporting structure, since such materials are readily available at modest cost and have a well established record in structural applications. Hoop wound tubes appear to be a desirable structural form, since the intended application is reminiscent of various pressure vessel design problems. However the asymmetric nature of the internal pressure loading markedly affects the utility of highly anisotropic materials in this application. Although circumferentially wound composite tubes can provide large strength factors of safety for high pressure launchers, they may represent a very poor material axes orientation from a structural stiffness point of view. This fact is illustrated in Table 1, which provides results of two dimensional static analyses of the finite element model shown in Figure 2, representing one quadrant of the round bore launcher depicted in Figure 1. The table compares predicted rail deflections for the subject structure under a rail surface pressure loading of 345 MPa for alternative inner supporting structure material types and material axes orientations. Structural dimensions, material properties, and other details of the finite element models are provided in Appendix 1. It should be noted that the material interfaces present in this finite element model and those which follow are modeled using interface elements based on a Coulomb friction constitutive law. The significance of these interfaces in launcher structural design is discussed by Fahrenthold et al. (1988a).

The Table 1 results indicate that since circumferentially wound composite structures effectively resist hoop elongation but not shape distortion, they perform poorly in the intended application. A vertical fiber orientation more closely aligns the high modulus material axis with applied load and hence reduces rail deflections. By extension the modeling results suggest the importance of material isotropy under the asymmetric pressure loading conditions, which lead to large in plane shear stresses and sharp spatial variations in principal stress axis orientations. With isotropic properties and a Young's modulus one third higher than that of steel, ceramic (Al_2O_3) appears to be an attractive material choice for the inner supporting ring.

TABLE 1

MATERIAL TYPE	RAIL DEFLECTION (mm)
Ceramic (Al_2O_3)	0.230
Composite (IM6, vertical fibers)	0.593
Composite (IM6, radial fibers)	0.711
Composite (IM6, circumferential fibers)	0.923
Composite (E-glass, circumferential fibers)	1.490

Table 1. Rail surface deflection (at point A in Figure 1) as a function of the inner supporting structure material type, for the round bore launcher described in Appendix 1.

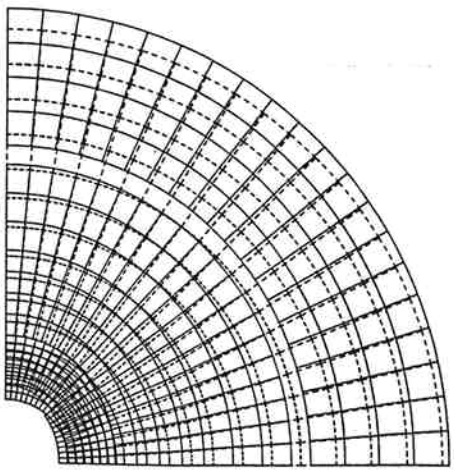

Figure 2. Original and displaced mesh for a finite element model of the round bore launcher shown in Figure 1 (ceramic inner ring) for static response under rail surface pressure loading.

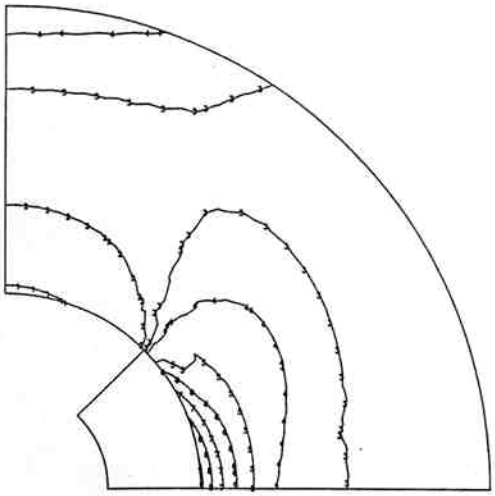

Figure 3. Contour plot of the maximum principal stress distribution in a ceramic inner supporing ring under rail surface pressure loading (contour interval = 40 MPa).

The preceding evaluation of elastic stiffness properties assumes that strength constraints can be satisfied. These constraints take the form of material specific failure modes whose effect on overall safety factors depends not only on the applied load but also on the manner in which the component materials distribute that load. Consider again the results of the static finite element analysis of the representative round bore model of Figure 1. Figure 3 shows a contour plot of the maximum principal stress developed in a ceramic inner support structure under rail surface pressure loading. In view of the low tensile strength of most ceramics, the contour plot suggests that tangential normal stress failure at a point directly beneath the sidewall centerline (point B in Figure 1) represents the primary structural failure mode for this design. Hence the use of ceramics introduces a rather demanding structural preloading constraint, accomodated in the interest of avoiding the dramatically inferior stiffness properties of fiber reinforced composite designs.

Table 2 shows the effect of changes in material type and orientation on the tangential normal stress developed at point B in Figure 1 in both preloaded and statically loaded configurations. In this case preloading has been applied by shrink fit assembly of an outer steel tube onto the inner support structure. Note that the stress response to the chosen preloading scheme is a strong function of the material type and orientation. This particular preloading technique is well suited to a ceramic design and can provide a compressive stress bias sufficient to avoid tensile failure of high quality ceramic under the design load (Fahrenthold et al., 1988a).

Analytical study of proposed composite designs invloves considerable post-processing of finite element modeling results to consider all potential yielding modes and material axes orientations. In general the spatially inhomogeneous stress state developed in the inner support structure makes it difficult to avoid some form of yielding in a composite design, nominally demanding an elastic-plastic stress analysis. For example the relatively low transverse yield strength of even high quality carbon fiber reinforced plastic (IM6) can lead to yielding of hoop wrap designs under the large bearing stress developed beneath the rails. The alternative vertical fiber orientation is subject to transverse normal stress yielding as well, in this case near the rail-sidewall interface, as indicated in the contour plot of Figure 4. In addition the presence of mutiple potential failure modes for composites tends to preclude the effective use of the simple stress bias preloading technique applied for the ceramic. In fact the minimal preloading needed to close assembly clearances may itself lead to material failure problems in composites, such as those encountered by Davidson et al. (1986) in the construction of a large bore fiber wound railgun. Although more complex cross ply layups and associated yield criteria deserve further study, the preceding strength constraints combine with the relatively low stiffness properties of composite rings to discourage the use of such materials when alternative design choices are available. The competing alternative of a laminated steel design is currently under study and will be discussed in a later section.

Rails, sidewalls, and outer supporting structure

Although the inner support structure largely determines the mechanical efficiency of a particular electromagnetic launcher design, some salient features of the remaining component parts deserve similar attention in view of their effect on structural performance.

As previously indicated, the presence of an outer support structure provides secondary containment, preloading capabilities, and longitudinal bending stiffness for devices which may exceed ten meters in length. The function and loading of this part contrast sharply with those of the inner support structure, dictating different material selection criteria. The outer support structure is often well insulated from the mechanical effects of the bore loading, due to the frequent presence of a frictional interface separating the inner and outer supporting structures and due to the obvious desire to make the inner support structure as stiff and massive as possible. As a result, finite element analyses have shown that the outer support structure tends to see a rather uniform internal pressure load, developed largely during the preload process invariably required to close assembly clearances. This is particularly true for steel tube outer structures of the type used to preload ceramic, since eddy current effects require that such tubes be located one and a half or more bore diameters from the back suface of the rail. With magnetic pressure loading effects on the outer structure typically second order perturbations from the preloaded state, hoop wound composite tubes can be effectively employed in a secondary containment role. However their use in applying large preload pressures to ceramic inner structures is again hindered by bearing stress limits transverse to the fiber direction and a restricted thermal operating range for shrink fit assembly procedures.

Although sidewalls have been essentially ignored as structual support members, numerical simulations have shown that if preloads are sufficiently high and the inner support structure is sufficiently stiff, bore deflections can be reduced significantly with the introduction of high modulus sidewall material. Considering the electrical insulating function of the sidewalls, ceramic is an attractive choice as a high modulus sidewall material. To date it has not been employed in this role, due to several factors. First, it is difficult to manufacture high quality ceramic sidewalls several meters in length, suggesting the need to introduce lateral seams in or near the bore surface. Second, sidewalls are often subject to projectile gouging or ablation, encouraging the conventional use of less expensive low modulus polycarbonates. Third, the difficulty of preloading low tensile strength ceramic parts tends to increase with increasing complexity of the part geometry and loading conditions. Recognizing these complications, a laminated steel design of the type discussed in the next section may be required in order to take advantage of the benefits of high modulus sidewalls.

Rail materials selection is of course strongly influenced by electrical design considerations. However with the development of

TABLE 2

MATERIAL	STRESS UNDER PRELOAD (MPa)	STRESS UNDER STATIC LOAD (MPa)
Ceramic (Al_2O_3)	-154.0	+229.0
Composite (IM6, vertical fibers)	-147.0	+670.0
Composite (IM6, radial fibers)	- 32.7	+ 74.7
Composite (IM6, circumferential fibers)	- 20.6	+673.0
Composite (E-glass, circumferential fibers)	- 24.0	+299.0

Table 2. Tangential normal stress at point A in Figure 1 as a function of inner supporting structure material type, for the round bore launcher described in Appendix 1.

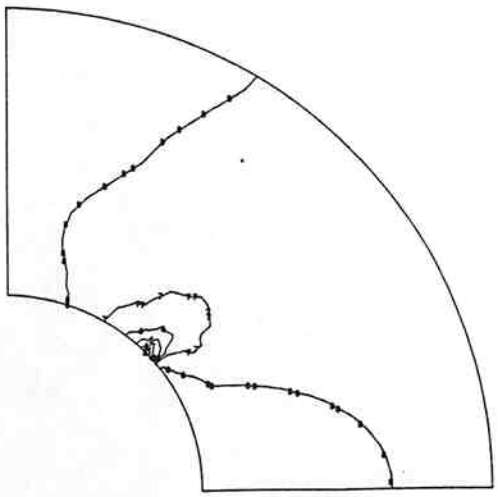

Figure 4. Contour plot of the distribution of the normal stress component transverse to the fiber direction in a composite (IM6) inner supporing ring under rail surface pressure loading (contour interval = 40 MPa).

TABLE 3

MATERIAL TYPE	RAIL SURFACE DEFLECTION (mm)	RAIL BASE DEFLECTION (mm)
Copper	0.230	0.151
Molybdenum	0.164	0.139

Table 3. Rail surface (point A in Figure 1) and rail base (point C in Figure 1) displacements as a function of rail material type, for the round bore ceramic-steel structure described in Appendix 1.

very stiff structural designs the importance of the rail's role as a structural member has increased. Table 3 compares predicted displacements of the rail surface and rail base (points A and C in Figure 1) under static loading for the ceramic-steel design of Appendix 1, for both copper and molybdenum rails. The tabulated data indicates that a substantial portion of the bore surface deflection observed in high performance launchers can be attributed to rail deformation. Hence a significant incremental reduction in bore deflections is achieved by replacing conventional copper rails with high modulus conductors such as molydenum. It will be shown that the latter substitution may be mandated by the significant effects of Joule heating on the strength of the candidate materials.

Lightweight railgun design

The preceding discussion has focused on the development of laboratory based launchers, designed for maximum stiffness under rather permissive weight or cost constraints. It has been shown that properly preloaded ceramic-steel systems can substantially outperform composite-steel railgun designs in this role. However the development of lightweight, low cost electromagnetic launchers demands a different design approach, since substantial reductions in the size and weight of the outlined laboratory based design require the development of improved structural ceramics. Recognizing the limitations of fiber reinforced composite designs, a new railgun concept has been suggested (O'Hara and Cascio, 1987) which employs a laminated steel construction to limit the development of eddy currents in the conducting inner support structure. If thin steel plates stacked to form an inner support structure can be insulated from each other and from the rails by very thin nonconducting epoxy or composite layers, it is in principle possible to build an inexpensive, high tensile strength, high modulus inner support structure and thereby decrease the cost and weight of high performance launchers. Such a lightweight design concept would probably incorporate a composite outer shell for preloading and logitudinal stiffness. Preloading might involve the pressurized injection of epoxy between the inner and outer support structures, fiber winding a composite tube onto the assembled laminations, or the use of a thermal shrink fit. The stress preloading achievable with these techniques is limited by the the previously outlined shortcomings of composites as well as the potential for plastic extrusion of solidified epoxy at high operating pressures.

Figure 5 depicts a two dimensional finite element model of a laminated steel launcher design. Dimensions and material properties used in the analysis are provided in Appendix 2. Note that the use of structural laminations fabricated from high tensile strength material makes it possible to construct a monolithic sidewall-inner support structure, in effect taking advantage of one of the significant benefits offered by high modulus sidewall designs. Figure 6 provides a contour plot of the von Mises stress field (Shigley and Mitchell, 1983) developed in the steel laminations for the case of static bore pressure loading at 345 mPa. As compared to the previous models, the reduced size and modified sidewall-support ring geometry intensifies the stress concentration developed in the support structure and shifts its position away from the sidewall centerline. Although the predicted maximum von Mises stress of 1502 MPa falls within an allowable range only for ultrahigh strength steel (4340), the proposed design concept is quite promising in view of the large weight savings it may offer. A disadvantage of the proposed design is the lack of convenient maintenance access, since none of the outlined preloading schemes appear to be reversible, a rather unique property of hydraulically preloaded ceramic-steel prototypes currently under development (Fahrenthold, 1988). This loss is somewhat compensated for by the relatively low cost of the component materials employed. Rail deflection for the outlined design (0.343 mm) is comparable to that achieved in the ceramic-steel structure previously described, with a factor of four reduction in total structural weight.

Size and weight reductions beyond those suggested by the outlined laminated design would appear to require shape optimization or rail thickness reductions, since direct support of the rail structure by an essentially steel frame is not likely to be improved upon from a materials selection point of view. Since the difficult question of shape optimization falls outside the scope of this paper, the following sections consider thermoelectrical limits to rail thickness reductions as a function of conducting material type.

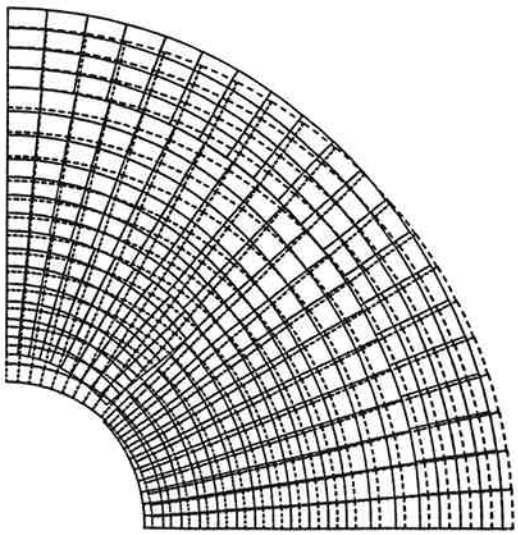

Figure 5. Original and displaced mesh for a finite element model of the round bore launcher shown in Figure 1 (laminated steel inner ring) for static response under rail surface pressure loading.

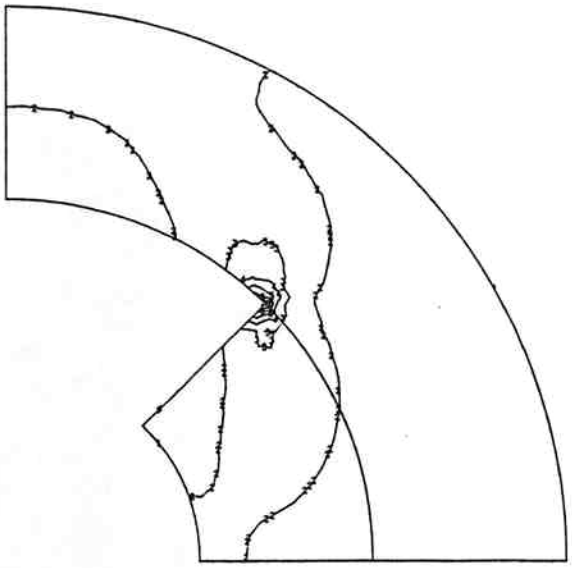

Figure 6. Contour plot of the von Mises stress distribution in a steel inner supporing ring under rail surface pressure loading (contour interval = 200 MPa).

ELECTRICAL DESIGN

Joule heating effects

The cross sectional dimensions of the conducting rails are often determined on the basis of conservative resistive heating calculations. However rail thickness reductions offer a means of reducing structural weight without stiffness penalties, since they effectively replace rail cross section with structural reinforcement located in close proximity to the applied load. For this reason a closer examination of the Joule heating effect is of significant structural interest.

As previously mentioned, no general model of the nonlinear three dimensional railgun current diffusion problem has been developed, although one recent report has described development work on two dimensional finite element codes capable of predicting Joule heating effects in high performance launchers (Schnurr, 1987). Since such modeling capabilities are not yet generally available to systems designers, the discussion which follows considers a one dimensional nonlinear analysis of coupled heat and current diffusion in conductors of finite thickness, suitable for approximate evaluations of materials selection effects on structural performance (Kidder, 1959). This design approach is analagous to the use of classical linear one dimensional isothermal "skin depth" analyses to approximately size conductors for a variety of busbar and transmission line geometries (Hayt, 1974).

Consider a flat plate fabricated from a good electrical conductor, of finite thickness "h" but infinite in lateral extent, as depicted in Figure 7. The lower surface of the plate is the plane y=0 in the Cartesian coordinate system shown in the figure. Assume that a time dependent magnetic field intensity of magnitude H(t) and aligned with the x axis is imposed on the lower surface of the flat plate, while the magnetic field intensity along the upper surface of the plate is identically zero. Neglecting displacement currents in the conductor, Ampere's circuital law gives the resulting total current which flows in a segment of the plate of width "w" as (Long, 1987)

$$I(t) = H(t)\, w \tag{1}$$

where "w" is measured parallel to the plate surface and the current flows in the z direction. Given a rail current I(t) and characteristic rail dimensions "h" and "w", solution of the one dimensional heat diffusion and time varying Maxwell equations in the infinite plate conductor just described provides a qualitative comparison of the thermo-electromagnetic performance of candidate rail materials.

Field equations and boundary conditions

The field equations and constitutive relations for the outlined problem may be written as

$$J = -\partial H/\partial y \; ; \; -B = \partial E/\partial y \tag{2a,b}$$

$$\partial U/\partial t = (1/\rho)E^2 + \partial[k(\partial T/\partial y]/\partial y \tag{2c}$$

$$E = \rho J \; ; \; B = \mu H \; ; \; U = cT \tag{3a,b,c}$$

where J is the current density, B is the magnetic flux density, E is the electric field intensity, ρ is the resistivity, μ is the magnetic permeability, T is the temperature, U is the internal energy per unit volume, k is the thermal conductivity, and c is the specific heat per unit volume. The conductor density has been assumed constant, which is significant here only in that it excludes phase change effects. Rearrangement of the preceding expressions yields two nonlinear equations which govern heat and current diffusion in the conductor

$$\partial H/\partial t = (\rho/\mu)\, \partial^2 H/\partial y^2 + (\rho'/\mu)\, (\partial T/\partial y)\, (\partial H/\partial y) \tag{4}$$

$$\partial T/\partial t = [k/(c+c'T)]\, \partial^2 T/\partial y^2 + [\rho/(c+c'T)]\, (\partial H/\partial y)^2 + (k'/c)\, (\partial T/\partial y)^2 \tag{5}$$

where the magnetic permeability was assumed constant and the remaining material properties were taken to vary linearly with temperature in the form

$$\rho = \rho_o + \rho' T \; ; \; k = k_o + k'T \; ; \; c = c_o + c'T \tag{6a,b,c}$$

The latter expressions provide accurate descriptions of the behavior of copper and molybdenum between 20 ^{o}C and their respective melting temperatures.

The preceding field equations were integrated using the IMSL (1982) routine DPDES for boundary and initial conditions

$$H(0,t) = H_o \sin(\pi t/p) \; ; \; H(h,t) = 0 \tag{7a,b}$$

$$\partial T(y,t)/\partial y = 0 \text{ at } y=0,h \tag{8a,b}$$

$$H(y,0) = 0 \; ; \; T(y,0) = T_o \tag{9a,b}$$

where T_o is the ambient temperture and "p" is the time duration of a representative railgun current pulse input. Note that the insulated boundary condition applied to the thermal diffusion problem represents a conservative design assumption.

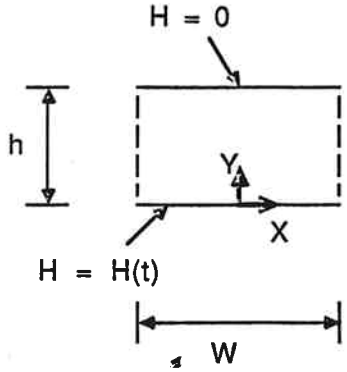

Figure 7. Geometry of the one dimensional coupled thermal and electromagnetic diffusion problem.

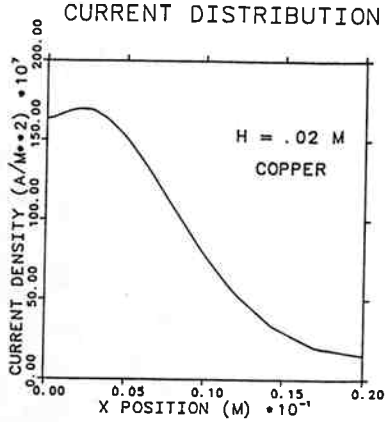

Figure 8. Predicted current density distribution in the plate of Figure 7, at t=p/2, for a copper conductor.

Simulation results

The preceding model may be used to estimate the effect of alternative rail material selections on temperature and current distributions which arise during high performance launcher operation. The parameter "w" is set equal to the rail perimeter in order to yield a surface current density in the one dimensional model identical to the average surface current density for the rail cross section of interest, while the parameter "h" is taken to be one half the actual rail thickness. The numerical parameters used in the simulations are provided in Appendix 3.

Figures 8 and 9 show current density and temperature distributions representative of the rail geometry used in the structural models previously discussed. Note that temperature effects in the nonlinear problem lead to nonmonotonic current density variations which differ from the approximately exponential current density decrease with depth predicted by linear isothermal simulations. Table 4 compares estimated maximum current densities in geometrically identical copper and molybdenum rails at t=p/2 as well as maximum temperatures in those rails at the end of the current pulse, for two different rail thicknesses. The results demonstrate that maximum operating temperatures decrease as rail thickness and electrical conductivity increase, as would be expected. Increased temperatures may in some cases be tolerated in the interest of improved structural stiffness, depending upon the temperature dependence of the candidate materials' elastic moduli (Budinski, 1983) as well as system power supply capacities.

With regards to strength constraints, this analysis provides an approximate basis for the determination of minimum allowable conductor thickness under transient current loads. If the design bore pressure exceeds the yield strength of the rail material at the maximum operating temperature predicted by this analysis, then plastic deformation of the rails can be expected to require honing or other reworking of the bore after each shot. A general conclusion is suggested by Budinski's (1983) discussion of the thermal properties of copper and molybdenum alloys. Softening of copper alloys at use temperatures above 200°C would appear to preclude their use in existing high performance launchers at rail half-thicknesses much below the typical 0.02 m shown in Table 4. With molybdenum alloys suitable for use in air at temperatures as high as 760°C, the Table 4 data indicates that such materials can permit large reductions in rail thickness, reducing structural weight and improving the launcher's specific stiffness.

CONCLUSION

The preceding analysis has considered the materials selection design considerations most important to the development of improved electromagnetic launcher structures. The design of high performance railguns should include consideration of material property variations on both mechanical and electrical performance. Although a nominal range of material choices exists for each of the component parts, feasible material combinations are restricted considerably by system design constraints.

Given a feasible material combination, quantification of the effects of rail loading, material anisotropy, resistive heating, assembly clearances, and other factors on the system performance calls for numerical modeling of both mechanical and electromagnetic effects. Such simulations allow estimates of performance trade-offs be made, in order to determine the cost, weight, durability, and other properties of designs based on various material selections. Based upon property data for commercially available materials and the numerical analyses presented here, it appears that laminated steel designs can achieve a factor of four or more reduction in electromagnetic launcher structural weight, as compared to existing laboratory devices. However such weight reduction may preclude convenient disassembly, and may demand the use of molybdenum alloys for rail fabrication in order to achieve structural stiffness equal to that provided by ceramic-steel designs. This result suggests that next generation electromagnetic launchers constructed for fixed installations and for vehicular mounting can be expected to differ substantially in material composition, yet offer comparable and significant stiffness improvements over conventional steel framed reinforced composite systems.

TABLE 4

RAIL TYPE	J_{max} (GA/m^2)	T_{max} (^oC)
Copper (h=0.02 m)	1.70	125
Molybdenum (h=0.02 m)	1.12	164
Copper (h=0.01 m)	2.65	228
Molybdenum (h=0.01 m)	2.55	522

Table 4. Maximum current density (at t=p/2) and maximum temperature (at t=p) as a function of rail thickness and material type, for the one dimensional model shown in Figure 7.

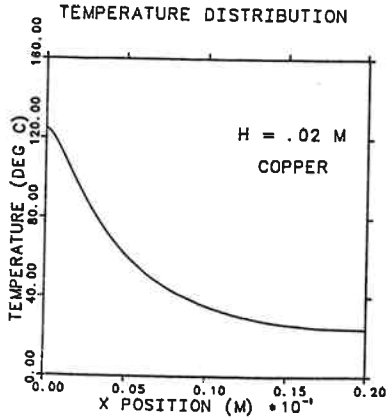

Figure 9. Predicted temperature distribution in the plate of Figure 7, at t=p, for a copper conductor.

ACKNOWLEDGEMENTS

This work was supported by the U.S. Army Armament Research, Development, and Engineering Center and the Defense Advanced Research Projects Agency. Computer time was provided by the University of Texas System Center for High Performance Computing.

REFERENCES

Brown, D. and Hamilton, E.P., 1984, Electromechanical Energy Conversion, Macmillan, New York.

Budinski, K.G., 1983, Engineering Materials - Properties and Selection, Reston Publishing Co., Reston, Virginia.

Davidson, R.F., Cook, W.A., Raburn, D.A., and Schnurr, N.M., 1986, "Predicting Bore Deformations and Launcher Stresses in Railguns," IEEE Transactions on Magnetics, Vol. MAG-22, No.6, pp. 1435-1440.

Hayt, W.H., 1974, Engineering Electromagnetics, McGraw-Hill, Inc., New York.

Hibbitt, Karlsson, and Sorensen, 1985, ABAQUS User's Manual.

Fahrenthold, E.P., Peterson, D.R., Price, J.H., and Wu, A.Y., 1988a, "Stress Analysis for Design of Electromagnetic Launchers," Journal of Vibration, Acoustics, Stress, and Reliability in Design, Vol. 110, No. 3, pp. 395-400.

Fahrenthold, E.P., Price, J.H., and Peterson, D.R., 1988b, "Structural Design of Cylindrical Railguns," Proceedings of the 4th Symposium on Electromagnetic Launch Technology, IEEE Transactions on Magnetics, in press.

Fahrenthold, E.P., 1988, "Design of Pressure Vessel Cascades for Electromagnetic Launchers," Quality Computer-Aided Engineering for Industry and Education, ASME PVP - Vol. 142, pp. 21-26.

IMSL Library Reference Manual, 1982, Edition 9, Vol. 1.

Johnson, W., ed., 1986, Proceedings of the 1986 Hypervelocity Impact Symposium, International Journal of Impact Engineering, Vol. 5.

Kidder, R.E., 1959, "Nonlinear Diffusion of Strong Magnetic Fields Into a Conducting Half Space," University of California Lawrence Radiation Laboratory Report #5467.

Long, G.C., 1987, "Fundamental Limits to the Velocitiy of Solid Armatures in Railguns," PhD thesis, Department of Electrical and Computer Engineering, University of Texas, Austin.

O'Hara, G.P., and Cascio, M., 1987, "Structural Integrity of Metallic Armature Rail Guns," Procceedings of the 5th U.S. Army Symposium on Gun Dynamics, T.E. Simkins and C.G. Homan, editors, The Institute on Man and Science, Rensselaerville, New York, 23-25 September, pp. 328-343

Schnurr, N.M., 1987, "Thermal Analysis of Electromagnetic Launcher Rails," Los Alamos National Laboratory Report #LA-11087-MS.

Shigley, J.E., and Mitchell, L.D., 1983, Mechanical Engineering Design, McGraw-Hill, Inc., New York.

Tsai, S.W., 1986, Composites Design - 1986, Think Composites, Dayton, Ohio.

Weldon, W.F., 1987, "Development of Hypervelocity Launchers," International Journal of Impact Engineering, Vol. 5, pp. 671-679.

APPENDIX 1

The static finite element calculations whose results are presented in Figures 2 through 4 and Tables 1 through 3 were performed for a structure of the type shown in Figure 1, with the following dimensions: bore radius = 0.045 m, rail thickness = 0.040 m, inner supporting ring thickness = 0.125 m, outer supporting ring thickness = 0.100 m, and interference fit (between the inner and outer supporting rings) = 0.00025 m. The chosen outer ring wall thickness is based upon detailed analysis of ceramic-steel launcher designs (Fahrenthold et al., 1988a).

Material properties used in the analysis were as follows: for the steel outer ring, E = 207.0 GPa, ν = 0.29; for the polycarbonate sidewalls, E = 11.59, GPa, ν = 0.25; for the copper rails, E = 107.6 GPa, ν = 0.355; for the molybdenum rails, E = 324.0 GPa, ν = 0.325; and for the ceramic inner ring, E = 276.0 GPa, ν = 0.22. The composites were modeled as transversely isotropic materials with the following properties (Tsai, 1986): for the IM6, E_1 = 203.0 GPa, E_2 = 11.20 GPa, ν_1 = 0.32, ν_2 = 0.50, shear modulus = 8.40 GPa; for the E-glass, E_1 =38.60 GPa, E_2 = 8.27 GPa, ν_1 = 0.26, ν_2 = 0.50, shear modulus = 4.14 GPa.

The numerical simulations employed the general purpose finite element code ABAQUS (Hibbitt, Karlsson, and Sorensen, 1985) with the structural model incorporating 407 elements and 2712 degrees of freedom and requiring up to two minutes of CPU time for static analysis on a Cray X-MP/24.

APPENDIX 2

The static finite element calculations whose results are presented in Figures 5 and 6 were performed for a structure of the type shown in Figure 1, with the following dimensions: bore radius = 0.045 m, rail thickness = 0.040 m, inner supporting ring thickness = 0.045 m, and outer supporting ring thickness = 0.025 m. A line fit (no interference) was assumed between the inner and outer supporting rings.

Material properties used in the analysis were the same as those listed in Appendix 1, however the monolithic sidewall and inner support structure was modeled as steel while the outer support ring was modeled as IM6.

APPENDIX 3

The electromagnetic modeling calculations whose results are presented in Figures 8 and 9 and Table 4 were performed for the one dimensional geometry shown in Figure 7 with $H_o = (3.20 \times 10^6)/w$ A/m, T_o = 20 ^oC, p = 0.0066 s, h = 0.020 and 0.010 m, and the following material properties (Long, 1987): for the copper, $\rho_o = 1.57 \times 10^8$ ohm-m, $\rho' = 0.00809 \times 10^8$ ohm-m/^oC, k_o = 401.0 W/(m-^oC), k' = -0.0655 [W/(m-^oC)]/^oC, $c_o = 3.10 \times 10^6$ J/(^oC-m^3), c' = 0.000864×10^6 [J/(^oC-m^3)]/^oC; for the molybdenum, $\rho_o = 5.65 \times 10^8$ ohm-m, $\rho' = 0.00288 \times 10^8$ ohm-m/^oC, k_o = 139.0 W/(m-^oC), k' = -0.0259 [W/(m-^oC)]/^oC, $c_o = 2.48 \times 10^6$ J/(^oC-m^3), c' = 0.000723×10^6 [J/(^oC-m^3)]/^oC. The parameter "w" was calculated as the perimeter of a rail of thickness "2h" and extending over a ninety degree arc of the bore. The magnetic permeability of both materials was taken to be that of free space ($4\pi \times 10^{-7}$ H/m).